

Reconnection of skewed vortices

Y. Kimura¹ and H. K. Moffatt^{2,†}

¹Graduate School of Mathematics, Nagoya University, Chikusa-ku, Nagoya 464-8602, Japan

²Department of Applied Mathematics and Theoretical Physics, University of Cambridge,
Wilberforce Road, Cambridge CB3 0WA, UK

(Received 6 November 2013; revised 4 February 2014; accepted 22 April 2014)

Based on experimental evidence that vortex reconnection commences with the approach of nearly antiparallel segments of vorticity, a linearised model is developed in which two Burgers-type vortices are driven together and stretched by an ambient irrotational strain field induced by more remote vorticity. When these Burgers vortices are exactly antiparallel, they are annihilated on the strain time-scale, independent of kinematic viscosity ν in the limit $\nu \rightarrow 0$. When the vortices are skew to each other, they are annihilated under this action over a local extent that increases exponentially in the stretching direction, with clear evidence of reconnection on the same strain time-scale. The initial helicity associated with the skewed geometry is eliminated during the process of reconnection. The model applies equally to the reconnection of weak magnetic flux tubes under the action of a strain field, when Lorentz forces are negligible.

Key words: Navier–Stokes equations, vortex flows, vortex interactions

1. Introduction

The reconnection of vortex filaments has been recently visualised in water in the brilliant experiment of Kleckner & Irvine (2013). These authors have succeeded in generating a vortex in the form of a trefoil knot, which is highly unstable. Figure 1 shows clips from the movie in the supplementary material to that paper. The upper row (*a–d*) shows the evolution of the trefoil vortex from a time shortly after its creation up to the moment of reconnection; the vortex is visualised by air bubbles, which are drawn to the pressure minimum in the vortex core. The clips show three regions where initially remote parts of the vortex are apparently swept into close proximity, generating three nearly antiparallel vortex pairs in these regions. The lower row (*e–h*) shows a close-up of one of these vortex pairs as it evolves; between the times of clips (*g*) and (*h*), a rapid reconnection, which may fairly be described as ‘explosive’, has occurred, with complicated distortion at the ends of the reconnecting region.

This situation as described by Kleckner & Irvine (2013) is represented schematically in figure 2. The more rapid propagation of the inner strands of the vortex generates three antiparallel vortex pairs that are necessarily slightly skewed. The stretching of

† Email address for correspondence: hkm2@damtp.cam.ac.uk

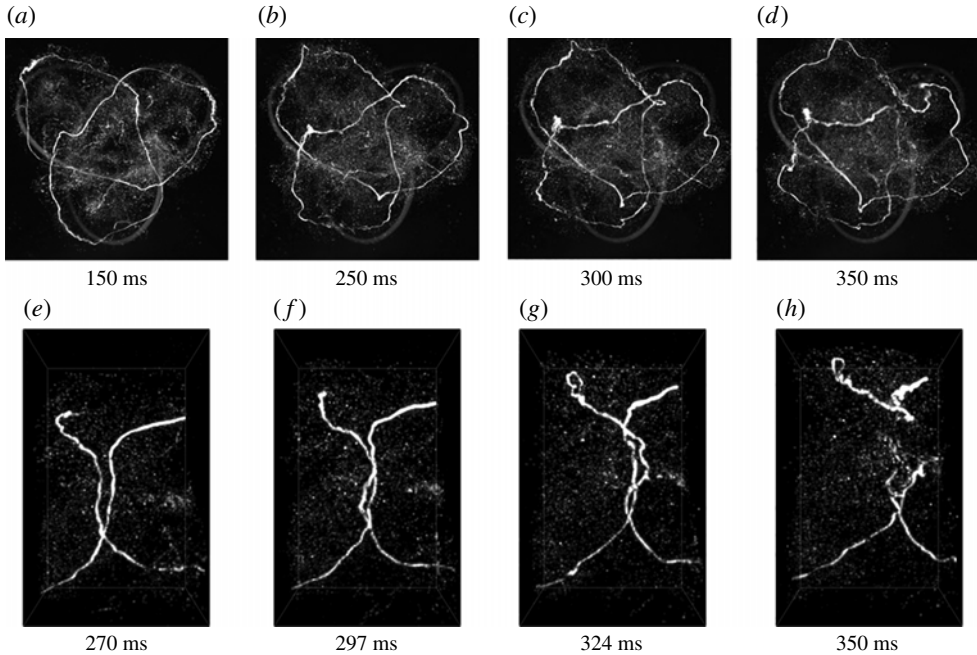


FIGURE 1. Reconnection of a trefoil vortex in water (reproduced from Kleckner & Irvine (2013), with permission). (a–d) Evolution of trefoil vortex through a reconnection event; the area shown is approximately $120 \text{ mm} \times 120 \text{ mm}$. (e–h) Zoom of upper right reconnection event, viewed from the side, which occurs between 324 ms and 350 ms; the area shown is approximately $38 \text{ mm} \times 61 \text{ mm}$.

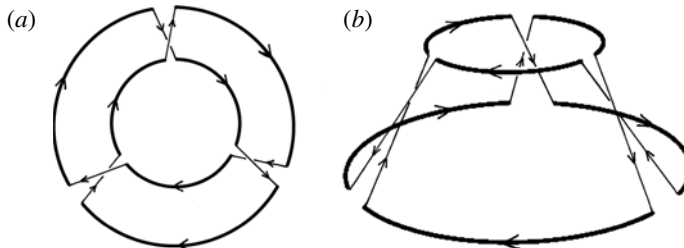


FIGURE 2. Schematic diagram of the trefoil vortex just before reconnection. Arrows indicate the direction of the vorticity. The plan view on (a), and side view on (b), show the three stretched, antiparallel, skewed vortex pairs, where reconnection will occur. At the instant considered, the upper ring propagates upwards more rapidly than the lower ring.

these vortex pairs due to the excess speed of the smaller ‘vortex ring’ is inevitably associated with an inflow to each pair, which rapidly gives rise to the explosive reconnection process. This is of course a highly idealised description; the actual flow as viewed in the movie has a high degree of irregularity, but the ultimate product of the trefoil reconnections does appear to be two vortex rings as indeed portrayed by figure 2.

Two length-scales characterise this type of flow, the geometric scale L of the initial trefoil knot, and the cross-sectional radius δ of the vortex core, i.e. the tubular region

in which the vorticity is essentially concentrated; outside this region, the flow is effectively irrotational. If the circulation of the vortex is Γ , then the induced velocity at any point near the vortex is of order $U_0 \sim \Gamma/L$, and the rate of strain at any such point is of order $\gamma_0 \sim \Gamma/L^2$. (This ignores the swirl component of velocity $\Gamma/2\pi r$ at small distance r from any element of the vortex, which does not contribute to motion of that element.) The vortex moves and is deformed under the action of the induced velocity and strain fields, locally like the familiar Burgers vortex; its cross-sectional scale is then given in order of magnitude by $\delta \sim (\nu/\gamma_0)^{1/2} \sim Re^{-1/2}L$, where $Re = \Gamma/\nu$ is the vortex Reynolds number, and ν is the kinematic viscosity of the fluid. We shall assume throughout that $Re \gg 1$, so that $\delta \ll L$. This condition was satisfied in the above experiment, for which the Reynolds number of the initial flow was in the range 10^3 – 10^4 . With $Re = 10^4$, and with $L \sim 10^{-1}$ m and $\nu \sim 10^{-6}$ m² s⁻¹ for water, the above estimates are $\delta \sim 1$ mm, $U_0 \sim 10^{-1}$ m s⁻¹, $\Gamma \sim 10^{-2}$ m² s⁻¹ and $\gamma_0 \sim 1$ s⁻¹.

Now let a be any intermediate scale satisfying $\delta \ll a \ll L$. Then in any sphere of radius a , centred at or near any point of the vortex, the rate of strain may be treated as approximately uniform. If we refer to the principal axes of strain, this strain field may be written as

$$\mathbf{U}_s = (-\alpha x, -\beta y, \gamma z), \quad (1.1)$$

where, by virtue of incompressibility, $\alpha + \beta = \gamma$, and we may suppose that $\alpha > 0$, $\gamma > 0$, $-\alpha \leq -\beta \leq \gamma$.

If $\beta > 0$ (the case of ‘extensive strain’), then any small material element of fluid is swept in towards the z -axis, and stretched in the $\pm z$ -directions. In this situation, if any two initially remote elements of the vortex happen to come within a distance $\sim a$ of each other in such a region of extensive strain, they will be swept in towards the z -axis and progressively aligned with it. It is this type of process that appears to be taking place in figure 1(e–h); the length of the nearly antiparallel segments revealed in this way is presumably $\sim a$. The explosive reconnection that occurs in passing from figure 1(g) to 1(h) can then be interpreted as due to the persistent sweeping of these antiparallel segments towards the z -axis. It is these considerations that motivate the simple model considered in the following sections.

For a general discussion of the background to this problem, see Pullin & Saffman (1998). In the turbulence context, attempts to represent turbulence as a random distribution of vortex tubes and/or sheets go back to Burgers (1948), Townsend (1951) and Rott (1958). Concentrated vortex filaments have been identified in many direct numerical simulations (DNS) of turbulence (e.g. Vincent & Meneguzzi 1991; Ishihara *et al.* 2007), and in the experiment of Douady, Couder & Brachet (1991) in which vortices were visualised by small air bubbles. Vortex reconnection was reviewed by Kida & Takaoka (1994), where an extensive list of references up to that date may be found. In particular, Saffman (1990) considered the reconnection of two antiparallel vortices confined to a plane and swept into close proximity by a strain field; he took partial account of the vortex–vortex interaction by noting that, as the vortex circulation is decreased, the axial pressure is locally increased, generating an axial flow that accelerates the effect of the imposed strain. Boratav, Pelz & Zabusky (1992) considered the interaction of skewed vortices, and to that extent their paper is more relevant to the present investigation; however, no strain field other than that induced by the local interacting vortices was imposed. For more recent investigations, see, for example, van Rees, Hussain & Koumoutsakos (2012) and Kudela & Kosior (2013).

The analogous problem of magnetic tube reconnection is treated in the monograph of Priest & Forbes (2000); simple models have been treated by Moffatt & Hunt

(2002) and Hattori & Moffatt (2005). For magnetic flux tubes, there is no counterpart of the ‘vortex–vortex’ interaction that is the most difficult aspect of the vortex reconnection problem. There is however a Lorentz force acting on the fluid that obviously influences the dynamics, but if the magnetic field is weak, this effect is negligible; in this limit, the magnetic reconnection model based on rapid distortion theory (RDT), as adopted in the following sections, is exact. For vortex reconnection, it is at best an approximation, most easily justified when the interacting vortices are exactly or nearly antiparallel, as appears to be the case for the reconnecting trefoil vortex.

2. Annihilation of Burgers vortices

For simplicity, we suppose that $\beta = \alpha$, and we first consider the action of the *axisymmetric* strain field

$$\mathbf{U} = (-\alpha x, -\alpha y, 2\alpha z), \quad \alpha > 0, \quad (2.1)$$

on a vorticity distribution $(0, 0, \omega(x, y, t))$. The vorticity is swept towards the z -axis and stretched in the $\pm z$ -directions. Within the context of RDT (Hunt & Carruthers 1990), the linearised vorticity equation is

$$\frac{\partial \omega}{\partial t} - \alpha x \frac{\partial \omega}{\partial x} - \alpha y \frac{\partial \omega}{\partial y} = 2\alpha \omega + \nu \left(\frac{\partial^2 \omega}{\partial x^2} + \frac{\partial^2 \omega}{\partial y^2} \right). \quad (2.2)$$

Here, the ‘self-interaction’ of the vorticity field is neglected in comparison with the sweeping and stretching effect of the uniform strain field (2.1). Actually there is a potential conflict between this RDT approximation and the assumption $Re \gg 1$ introduced above – see comment at the end of this section.

Equation (2.2) admits the well-known steady exact solution of the Navier–Stokes equations (Burgers 1948)

$$\omega_B(x, y) = (\Gamma/\pi\delta^2) e^{-r^2/\delta^2}, \quad \delta = \sqrt{2\nu/\alpha}, \quad (2.3)$$

where $r^2 = x^2 + y^2$, Γ is the circulation of the vortex and δ is its radial scale. If we place a vortex of this structure with its centreline at position $(0, y_0)$ at time $t=0$, then it will be swept towards the line $(0, 0)$, so that at time t its centreline is at $(0, Y(t))$, where $Y(t) = y_0 e^{-\alpha t}$. This moving vortex is still subject to the same uniform steady rate of strain α , and its vorticity field is therefore given by

$$\omega(x, y, t) = \omega_B(x, y - y_0 e^{-\alpha t}) = (\Gamma/\pi\delta^2) e^{-r_1^2(t)/\delta^2}, \quad (2.4)$$

where $r_1^2(t) = x^2 + (y - y_0 e^{-\alpha t})^2$. It may be verified directly that (2.4) satisfies (2.2); this is still an exact solution, but now of the *unsteady* Navier–Stokes equations, in conjunction of course with the background uniform strain. (For details concerning the more general non-axisymmetric situation, see appendix A; for extension of the Burgers solution to include axial velocity, see appendix B.)

When $Y(t) (= y_0 e^{-\alpha t}) \ll \delta$, we may expand (2.4) in Taylor series:

$$\omega_B(x, y - Y(t)) = \omega_B(x, y) - Y(t) \frac{\partial \omega_B(x, y)}{\partial y} + \frac{1}{2} Y(t)^2 \frac{\partial^2 \omega_B(x, y)}{\partial y^2} + \dots \quad (2.5)$$

Each term in this expansion is separately a solution of (2.2). In particular, the second term is

$$\omega_2(x, y, t) = (2y_0\Gamma/\pi\delta^4) e^{-\alpha t} y e^{-(x^2+y^2)/\delta^2}. \quad (2.6)$$

(Subsequent terms in the series, decaying as $e^{-n\alpha t}$, may be expressed in terms of Hermite polynomials $H_n(y)$.)

Suppose now that we have two vortices of equal and opposite circulations $\pm\Gamma$ with centrelines initially at positions $(0, \pm y_0)$. The solutions are additive (vortex–vortex interaction being neglected) so that now the required solution is

$$\omega(x, y, t) = \omega_B(x, y - y_0 e^{-\alpha t}) - \omega_B(x, y + y_0 e^{-\alpha t}) = \frac{\Gamma}{\pi\delta^2} (e^{-r_1^2(t)/\delta^2} - e^{-r_2^2(t)/\delta^2}), \quad (2.7)$$

where $r_{1,2}^2(t) = x^2 + (y \mp y_0 e^{-\alpha t})^2$. Again, this is an exact solution of (2.2); it is not however an exact solution of the Navier–Stokes equations, because of the RDT neglect of vortex–vortex interactions.

When $Y(t) = y_0 e^{-\alpha t} \ll \delta$, we may again expand (2.7) as a Taylor series, in which now only the terms odd in y survive; at leading order,

$$\omega(x, y, t) \sim 2\omega_2(x, y, t) = (4y_0\Gamma/\pi\delta^4) e^{-\alpha t} y e^{-(x^2+y^2)/\delta^2}. \quad (2.8)$$

This describes the exponential decay of vorticity (and this despite the persistent stretching) on a time-scale $\sim \alpha^{-1}$. It should be noted that, although this decay is caused by viscosity $\nu > 0$, the time-scale of decay is independent of ν in the limit $\nu \rightarrow 0$. It is in this sense that it may be considered to be a rapid, indeed explosive, process, which it seems appropriate to describe as one of ‘annihilation’ of vorticity.

The neglected vortex–vortex interaction probably makes little difference to this annihilation scenario. For so long as $Y(t)$ is still large compared with δ , this interaction merely provides an additional translational velocity $\Gamma/2Y(t)$ in the x -direction for the vortex pair. When $Y(t) \sim \delta$ or smaller, this translational velocity settles down to order Γ/δ ; at this stage, the interaction presumably leads to some shedding of vorticity into a wake region in the manner described by Buntine & Pullin (1989), but the persistent inflow towards the (x, z) -plane will cause continuing rapid annihilation of this shed vorticity also; indeed it seems likely that the shedding of vorticity will, if anything, accelerate the overall annihilation process. The enhanced-pressure mechanism of Saffman (1990) may also serve to accelerate the process; indeed in the Kleckner & Irvine (2013) experiment, the vortex in clips (a – d) of figure 1 evolves for a time ~ 200 ms, whereas the annihilation process from clips (g – h) occurs in less than 25 ms, evidently somewhat less than the strain rate time-scale.

3. Skewed Burgers vortices

Suppose now that at time $t = 0$ we place a Burgers-type vortex with straight centreline L_0 on the plane $y = y_0$ and tilted at an angle β_0 ($0 < \beta_0 < \pi/2$) to the z -axis; L_0 is given in parametric form by $(x_0, y_0, z_0) = (p \sin \beta_0, y_0, p \cos \beta_0)$, where p is a parameter on the line running from $-\infty$ to $+\infty$. The gradient of L_0 is $m_0 = x_0/z_0 = \tan \beta_0$. We assume that the irrotational strain field (2.1) advects and stretches this line, sweeping it towards the z -axis. At time t , the point initially at (x_0, y_0, z_0) has moved to $(X, Y, Z) = (x_0 e^{-\alpha t}, y_0 e^{-\alpha t}, z_0 e^{2\alpha t})$, so that the gradient of the line, now $L(t)$, in the (x, z) -plane at time t is

$$m = \tan \beta = X/Z = (x_0/z_0) e^{-3\alpha t} = e^{-3\alpha t} \tan \beta_0. \quad (3.1)$$

Let

$$\mathbf{e}(t) = (\sin \beta(t), 0, \cos \beta(t)), \quad (3.2)$$

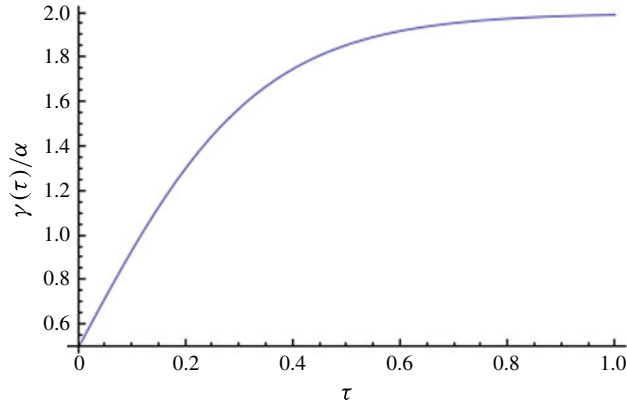


FIGURE 3. (Colour online) The effective stretch $\gamma(\tau)$ as a function of $\tau = \alpha t$, as given by (3.3) and (3.1), with initial condition $\beta_0 = \pi/4$. As τ increases, β decreases to zero, and $\gamma(\tau)$ rapidly asymptotes to 2α .

the unit vector directed along $L(t)$. Then the rate of stretch $\gamma(\tau)$ acting on the vortex at dimensionless time $\tau = \alpha t$ is

$$\gamma(\tau) = \mathbf{e} \cdot (\nabla \mathbf{U}) \cdot \mathbf{e} = 2\alpha s(\tau), \quad \text{where } s(\tau) = \frac{1}{2}(3 \cos^2 \beta(\tau) - 1), \quad \tau = \alpha t. \quad (3.3)$$

We may suppose that $\beta_0 < \cos^{-1}(1/\sqrt{3}) \approx 55^\circ$, so that $\gamma(\tau) > 0$ for all $\tau > 0$. Figure 3 shows the time variation of γ starting from an initial slope $\beta_0 = \pi/4$ (so $\gamma(0)/\alpha = 0.5$). For large τ , γ rapidly asymptotes to 2α ; in fact, $\gamma - 2\alpha \sim -3\alpha e^{-6\tau}$.

Under the basic assumption $Re \gg 1$, the response of the vortex to this changing rate of stretch is quasi-static; the radial scale $\sigma(t)$ of the vortex adapts accordingly, and is given by

$$\frac{1}{\sigma(t)^2} = \frac{\gamma}{4\nu} = \frac{\alpha}{2\nu} s(\tau) = \frac{1}{\delta^2} s(\tau). \quad (3.4)$$

Note that, although the strain field is not axisymmetric about the direction of $\mathbf{e}(t)$, the vortex itself at leading order (for $\Gamma/\nu \gg 1$) remains axisymmetric about this direction, according to the asymptotic analysis of Moffatt, Kida & Ohkitani (1994).

Now the perpendicular distance r_p from any point $\mathbf{x} = (x, y, z)$ to the line $L(t)$ is given by

$$r_p^2(\mathbf{x}, t) = (x \cos \beta(t) - z \sin \beta(t))^2 + (y - Y(t))^2, \quad (3.5)$$

where still $Y(t) = y_0 e^{-\alpha t}$. The Burgers-type vortex centred on $L(t)$ may then be expected to have time-dependent vorticity field

$$\boldsymbol{\omega}_1(\mathbf{x}, t) = \frac{\Gamma}{\pi \sigma(t)^2} \exp \left[-\frac{r_p^2(\mathbf{x}, t)}{\sigma(t)^2} \right] \mathbf{e}(t) = \frac{\gamma(t)\Gamma}{4\pi\nu} \exp \left[-\frac{\gamma(t)r_p^2(\mathbf{x}, t)}{4\nu} \right] \mathbf{e}(t), \quad (3.6)$$

where $\mathbf{e}(t)$, $\gamma(t)$ and $r_p(\mathbf{x}, t)$ are given by (3.2), (3.3) and (3.5), respectively.

Unlike (2.4), this is not an exact solution of the Navier–Stokes equation, but it provides a leading-order approximation for the evolution of the vortex when $Re \gg 1$. Note that, for large t , when $\beta(t) \rightarrow 0$, the solution approaches the exact solution (2.4) of the Navier–Stokes equation, so the field (3.6) becomes increasingly accurate as a solution of this equation, as time increases.

Now, just as in §2, we can superpose two solutions. We place a second vortex with circulation $-\Gamma$, centreline on the plane $y = -Y(t)$ and directed along $\mathbf{e}' = (-\sin \beta, 0, \cos \beta)$, and with the same Burgers-type cross-sectional structure; this is in effect the ‘chopsticks model’ of Kimura & Koikari (2004). For the second vortex, the vorticity field is

$$\boldsymbol{\omega}_2(\mathbf{x}, t) = -(\gamma \Gamma / 4\pi\nu) \exp(-\gamma r_p'^2 / 4\nu) \mathbf{e}', \tag{3.7}$$

with

$$r_p'^2 = (x \cos \beta(t) + z \sin \beta(t))^2 + (y + Y(t))^2. \tag{3.8}$$

The two vortices are now swept towards each other and overlap in a slicing scissor movement on the plane $y = 0$. The z -components of vorticity annihilate on the z -axis in a neighbourhood of $z = 0$ (that increases as $e^{3\tau}$), just as in §2 above, resulting in reconnection of the vortex tubes. The combined solution is given by $\boldsymbol{\omega}(\mathbf{x}, t) = \boldsymbol{\omega}_1(\mathbf{x}, t) + \boldsymbol{\omega}_2(\mathbf{x}, t)$. With dimensionless variables

$$(\hat{x}, \hat{y}, \hat{z}, \hat{Y}, \hat{y}_0) = \delta^{-1}(x, y, z, Y, y_0), \tag{3.9}$$

this is given by

$$\begin{aligned} & \frac{\pi \delta^2 \boldsymbol{\omega}(\hat{x}, \hat{y}, \hat{z}, \tau)}{\Gamma s(\tau)} \\ &= \exp\{-s(\tau)[(\hat{x} \cos \beta - \hat{z} \sin \beta)^2 + (\hat{y} - \hat{Y})^2]\}(\sin \beta, 0, \cos \beta) \\ & \quad - \exp\{-s(\tau)[(\hat{x} \cos \beta + \hat{z} \sin \beta)^2 + (\hat{y} + \hat{Y})^2]\}(-\sin \beta, 0, \cos \beta), \end{aligned} \tag{3.10}$$

from which contours $|\boldsymbol{\omega}(\hat{\mathbf{x}}, \tau)| = \text{const.}$ may be readily drawn.

Figure 4 shows two views of these contours, at the initial instant $\tau = 0$ and at a later (dimensionless) time $\tau = 0.63$. The initial separation $y_0/\delta = 1.356$ is chosen so that reconnection is just beginning (as indicated by the presence of the ‘bridge’ of vorticity magnitude in the lower view – see Kida & Takaoka (1987), Melander & Hussain (1989) and Kida & Takaoka (1994)). By the time $\tau = 0.63$, reconnection is already well advanced.

An alternative view of the bridge phenomenon is shown in figure 5. The appearance is extremely sensitive to the contour levels chosen. Here, as in figure 4, the contour surfaces $|\boldsymbol{\omega}(0, \hat{y}, 0, 0)|/|\boldsymbol{\omega}_{\max}(0, \hat{y}, 0, 0)| = 0.85$ and 0.95 are shown at time $\tau = 0$; the former is bridged but not the latter. An instant later at time $\tau = 0.1$, this bridge has disappeared, but it is still present at the lower contour level 0.75 , as shown in figure 5(c).

We may formalise the definition of a bridge in terms of an arbitrary threshold k ($0 < k < 1$): we shall say that the vortices are ‘ k -bridged’ if, on the line $x = z = 0$, $|\boldsymbol{\omega}|$ is minimal as a function of y at $y = 0$, but its value there is greater than $k|\boldsymbol{\omega}|_{\max}$. The larger the value of k , the stronger the bridge. Thus, for example, at time $\tau = 0$, the vortices of figure 5 are 0.85 -bridged but not 0.95 -bridged, while at time $\tau = 0.1$, they are 0.75 -bridged but not 0.85 -bridged.

Obviously, if two vortices are k -bridged, then they are also k' -bridged for any $0 < k' < k$. We may say that they are ‘strongly bridged’ if they are at least 0.5 -bridged. Figure 6 shows the function $|\boldsymbol{\omega}(0, \hat{y}, 0, 0)|$ for $\beta_0 = \pi/4$ and for three values of the initial separation \hat{y}_0 . The vortices are not strongly bridged for $\hat{y}_0 = 3$; as \hat{y}_0 is decreased (keeping $\beta_0 = \pi/4$ fixed), a (strong) bridge appears at $\hat{y}_0 \approx 2$; this bridge persists as \hat{y}_0 is further decreased, but the minimum at \hat{y} disappears when $\hat{y}_0 \approx 1$, and for $\hat{y}_0 < 1$ the bridge concept no longer applies.

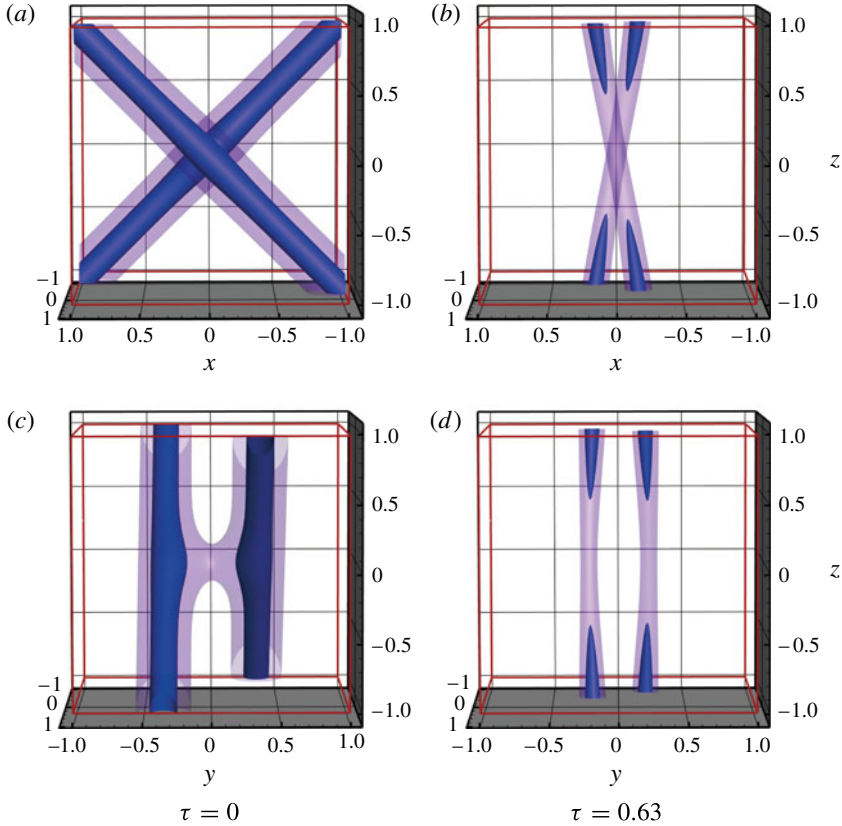


FIGURE 4. (Colour online) Skewed vortices offset in the y -direction (viewed in (a,b) the y -direction and (c,d) the x -direction) subjected to the straining flow (2.1) that aligns them onto the z -axis, showing unmistakable evidence of reconnection by the time $\tau = 0.63$. Contour surfaces are $|\omega|/|\omega|_{max} = 0.95$ (darker) and 0.85 (lighter). Parameter values: $\beta_0 = \pi/4$, $\hat{y}_0 = y_0/\delta = 1.356$. Note the ‘bridge’ in the lower view at $\tau = 0$, evidence of incipient reconnection.

Figure 7 shows the reconnection process for $\hat{y}_0 = 4$. In this case, no bridging is evident at $\tau = 0$ (although there is in fact a bridge at the extremely low threshold level $k = 0.0258$), and the vortices become nearly aligned and significantly overlapping by time $\tau = 2$. The z -axis is scaled by the factor $e^{-3\tau}$ in order to show how reconnection takes place over a range of z that, as indicated above, increases as $e^{3\tau}$.

The vortex lines given by (3.10) evidently lie in planes $y = \text{const}$. This means that the vorticity components can be expressed in terms of a ‘vorticity function’ $\chi(\hat{x}, \hat{y}, \hat{z}, \tau)$:

$$\omega(\mathbf{x}, t) = \frac{\Gamma}{2\sqrt{\pi}\delta^2} \left(\frac{\partial\chi}{\partial\hat{z}}, 0, -\frac{\partial\chi}{\partial\hat{x}} \right), \tag{3.11}$$

where, in fact,

$$\begin{aligned} \chi(\hat{x}, \hat{y}, \hat{z}, \tau) = & \sqrt{s(\tau)} \left[e^{-s(\tau)(\hat{y}+\hat{y})^2} \operatorname{erf} \left\{ \sqrt{s(\tau)}(\hat{x} \cos \beta + \hat{z} \sin \beta) \right\} \right. \\ & \left. - e^{-s(\tau)(\hat{y}-\hat{y})^2} \operatorname{erf} \left\{ \sqrt{s(\tau)}(\hat{x} \cos \beta - \hat{z} \sin \beta) \right\} \right]. \end{aligned} \tag{3.12}$$

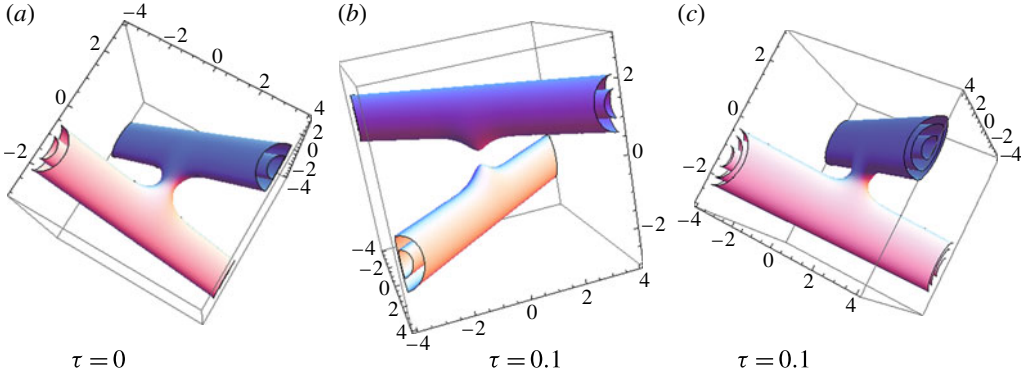


FIGURE 5. (Colour online) Contours of $|\omega|/|\omega_{max}|$ for same conditions as in figure 4. (a) Contour levels 0.85 and 0.95; the bridge is evident at the 0.85 level. (b) Same contour levels at $\tau = 0.1$, showing that the bridge has disappeared. (c) Contour levels 0.75, 0.85 and 0.95 at the same time $\tau = 0.1$, showing that the bridge is still present at the weaker level 0.75.

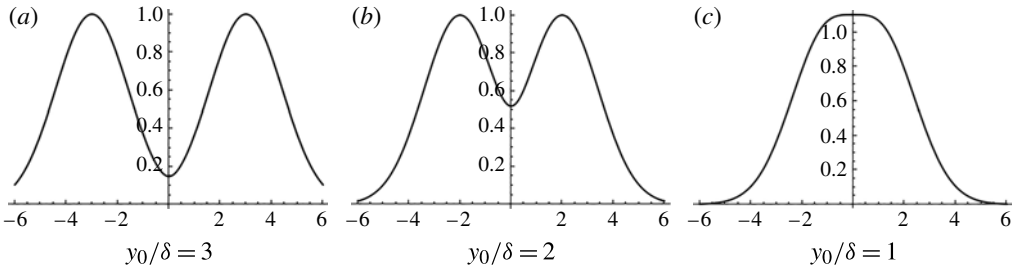


FIGURE 6. Plot of $|\omega(0, \hat{y}, 0, 0)|/|\omega_{max}(0, \hat{y}, 0, 0)|$ for $\beta_0 = \pi/4$ and for three values of the initial separation $\hat{y}_0 = y_0/\delta$. (a) At $|\omega(0, \hat{y}, 0, 0)| < 0.5 |\omega_{max}(0, \hat{y}, 0, 0)|$, there is no bridge at the $k = 0.5$ threshold. (b) At $|\omega(0, \hat{y}, 0, 0)| > 0.5 |\omega_{max}(0, \hat{y}, 0, 0)|$, a k -bridge exists with $k = 0.5$. (c) The minimum at $\hat{y} = 0$ has disappeared, indicating that for this initial separation the vortices significantly overlap and the bridge concept no longer applies.

Figure 8 shows a sample member of the family of surfaces $\chi = \text{const.}$, and of sections of seven members of the family by three planes $\hat{y} = 1, 0.25$ and 0 ; the lines of intersection are vortex lines of the flow in these planes.

The vorticity component ω_z as given by (3.11) is antisymmetric about the plane $y = 0$. Let

$$\Gamma_+(t) = \int_{y=0}^{\infty} \int_{x=-\infty}^{\infty} \omega_z \, dx \, dy, \quad (3.13)$$

the flux of vorticity over the half-plane $-\infty < x < \infty$, $y > 0$, i.e. from (3.10) in dimensional form,

$$\Gamma_+(t) = \frac{\gamma \Gamma \cos \beta}{4\pi\nu} \int_{y=0}^{\infty} \int_{x=-\infty}^{\infty} e^{-(\gamma/4\nu)x^2 \cos^2 \beta} [e^{-(\gamma(y-Y)^2/4\nu)} - e^{-(\gamma(y+Y)^2/4\nu)}] \, dx \, dy. \quad (3.14)$$

This integrates to give, on simplification,

$$\Gamma_+(t) = \Gamma \operatorname{erf}[Y(t)/\delta] \sim \Gamma \hat{y}_0 e^{-\tau} \quad \text{as } \tau \rightarrow \infty. \quad (3.15)$$

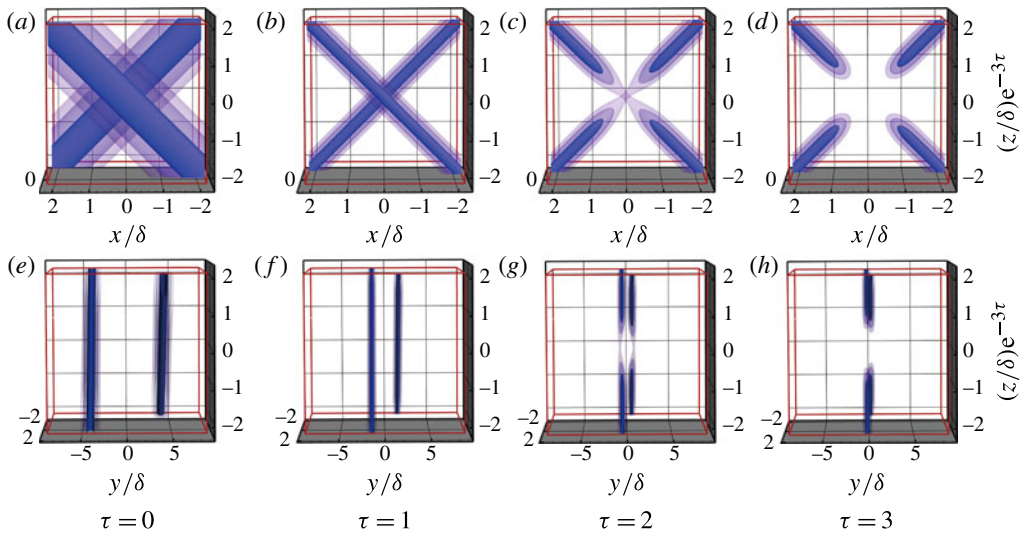


FIGURE 7. (Colour online) As in figure 4, but with $\hat{y}_0 = 4$. Here the z -coordinate is scaled by the factor $e^{-3\tau}$ in order to show that the field reconnects (with concomitant annihilation) for $\tau > 2$ over an extent of the z -axis that increases as $e^{3\tau}$.

Thus, the total circulation in the half-plane $y > 0$ decreases exponentially to zero as the reconnection proceeds. (Similarly, of course, for the flux of vorticity $\Gamma_-(t) = -\Gamma_+(t)$ over the half-plane $y < 0$.)

The neglected vortex–vortex interaction effect is a serious complicating factor, because vortices that are not parallel have a tendency to crank each other into double spirals in the region of closest approach. Actually, in the experiment of Kleckner & Irvine (2013), this interactive winding effect appears to be concentrated near the ends of the nearly antiparallel segments, where the vortex structure becomes quite convoluted after reconnection (see figure 1*h*). It again seems likely that, under the persistent action of the ambient strain, this interactive effect will, if anything, simply accelerate the reconnection process.

4. Helicity evolution during vortex reconnection

We can now address the interesting question of how the helicity of the vorticity distribution changes during the above type of reconnection process. We recall that, for a single knotted vortex tube of circulation Γ , the helicity is given by

$$\mathcal{H} = \Gamma^2(Wr + Tw), \quad (4.1)$$

where Wr is the writhe of the axis C of the vortex, and Tw is the twist, partly associated with the torsion of C and partly with ‘internal twist’ of the vortex lines within the vortex tube (Moffatt & Ricca 1992). The writhe Wr can be interpreted as the average over all projections of the sum of the (signed) crossings of the knot. For the trefoil knot created by Kleckner & Irvine (2013), $Wr = 3$, and after reconnection into two unlinked vortex rings, $Wr = 0$. Thus the writhe ingredient of helicity is changed as a result of vortex evolution. It is conceivable that some or all of this writhe helicity is converted to twist helicity during reconnection. We now investigate this possibility on the basis of the solution (3.10).

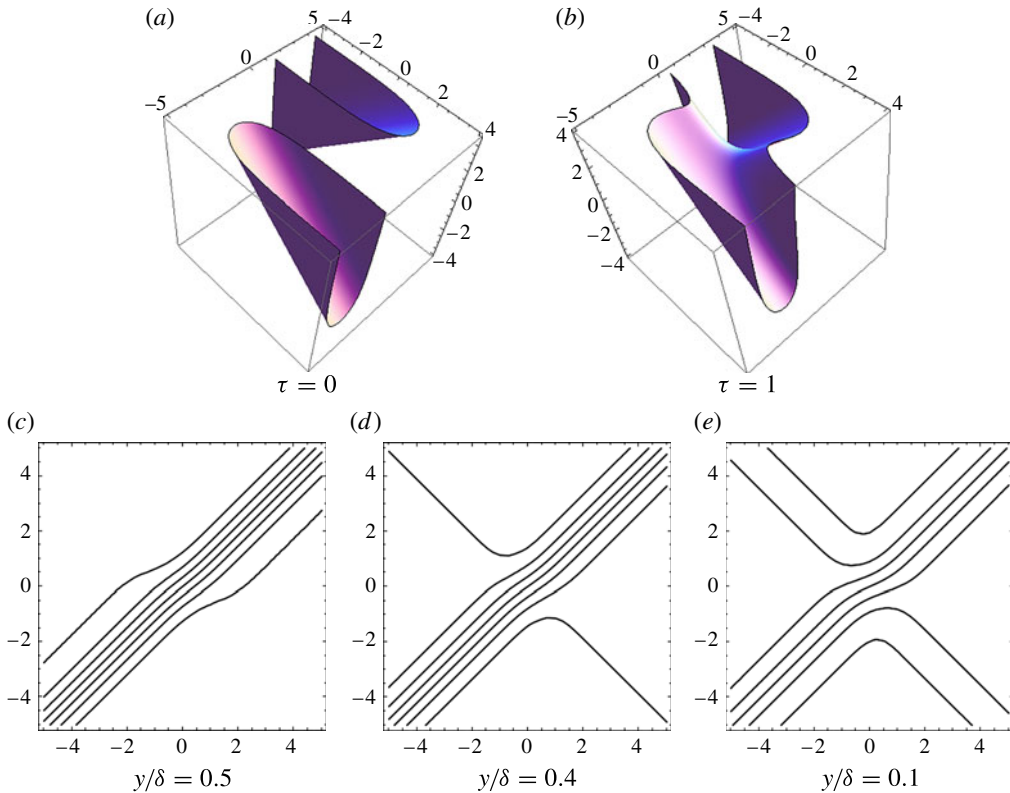


FIGURE 8. (Colour online) (a,b) Sample vortex surface $\chi = 0.3$ for $\hat{y}_0 = 3$ at two instants (a) before and (b) during reconnection. (c–e) Vortex lines at time $\tau = 1$ given as sections of surfaces $\chi = 0, \pm 0.2, \pm 0.4, \pm 0.6$, by planes $\hat{y} = \text{const.}$: (c) no reconnection is evident; (d) slight reconnection; (e) advanced reconnection. The abscissa in these plots is $\hat{x} \cos \beta(\tau)$ and the ordinate is $\hat{z} \sin \beta(\tau)$.

For the analogous problem of magnetic flux-tube reconnection, it has been argued by Wright & Berger (1989) that (magnetic) helicity is converted in this way (from writhe to twist) during reconnection, the total net helicity remaining nearly constant; this requires an appropriately ordered reconnection of ‘sub-tubes’, but it has never been convincingly established that this ordering is favoured by a natural diffusive process. The issue is important because the idea that magnetic fields relax in such a way as to minimise energy subject to conserved helicity (Taylor 1974) is one of the cornerstones of the magnetohydrodynamics of turbulent fusion plasmas.

We start from the consideration that, for the two skewed vortices considered above, even without axial flow in either vortex, there is an interaction (or ‘writhe’) helicity arising from the fact that the velocity induced by either vortex has a non-zero component parallel to the other. It is easiest to consider the interaction of a steady Burgers vortex B_0 (with vorticity ω_0 and associated velocity \mathbf{u}_0) as given by (2.3), and a second Burgers vortex $B_1(\omega_1, \mathbf{u}_1)$ as described by (3.6). Consider first the initial situation when, at time $t = 0$, the vortices are well separated, i.e. $y_0 \gg \delta$, and suppose that the vortices have circulations $\pm \Gamma$, respectively. With $r^2 = x^2 + y^2$, the velocity

field for $r \gg \delta$ due to B_0 is just that due to a concentrated line vortex, i.e.

$$\mathbf{u}_0(\mathbf{x}) = (\Gamma/2\pi r^2)(-y, x, 0), \quad (4.2)$$

and this is approximately constant on any cross-section $p = \text{const.}$ of B_1 . So, on B_1 ,

$$\mathbf{u}_0 = (\Gamma/2\pi)(p^2 \sin^2 \beta + y_0^2)^{-1}(-y_0, p \sin \beta, 0); \quad (4.3)$$

hence, with $\mathbf{e} = (\sin \beta, 0, \cos \beta)$,

$$\mathbf{u}_0 \cdot \mathbf{e} = (-\Gamma y_0 \sin \beta / 2\pi)(p^2 \sin^2 \beta + y_0^2)^{-1}, \quad (4.4)$$

and so, integrating first over the cross-section of B_1 , then along its axis,

$$\int_{B_1} \mathbf{u}_0 \cdot \boldsymbol{\omega}_1 dV = \frac{\Gamma^2 y_0 \sin \beta}{2\pi} \int_{-\infty}^{\infty} \frac{dp}{p^2 \sin^2 \beta + y_0^2} = \frac{\Gamma^2}{2}. \quad (4.5)$$

By symmetry, we have a similar result for the integral over B_0 , and hence the total initial helicity is

$$\mathcal{H} = \int \mathbf{u} \cdot \boldsymbol{\omega} dV = \Gamma^2, \quad (4.6)$$

the integral now being over all space. Note that this helicity is determined solely by the instantaneous vorticity distribution and is unaffected by the presence of the background irrotational strain. It admits interpretation as the writhe helicity (Moffatt & Ricca 1992), there being one crossing viewed from all projections (except a set of measure zero). If the sign of circulation of one of the vortices is changed, then of course the helicity changes sign also.

As the vortex B_1 is swept towards B_0 by the strain field, this helicity remains constant until the separation $Y(t)$ reduces to $O(\delta)$. We may calculate the helicity as a function of the dimensionless time $\tau = \alpha t$ as follows. The velocity \mathbf{u}_0 induced by the vortex B_0 is

$$\mathbf{u}_0(\mathbf{x}) = (\Gamma/2\pi r^2)(1 - e^{-r^2/\delta^2})(-y, x, 0), \quad (4.7)$$

which of course asymptotes to (4.2) for $r \gg \delta$, and the vorticity field $\boldsymbol{\omega}_1(\mathbf{x}, t)$ of B_1 is (from (3.6))

$$\boldsymbol{\omega}_1(\mathbf{x}, t) = \frac{\gamma(t)\Gamma}{4\pi\nu} \exp\left[-\frac{\gamma(t)r_p^2(\mathbf{x}, t)}{4\nu}\right] \mathbf{e}(t), \quad (4.8)$$

where $\mathbf{e}(t)$, $\gamma(t)$ and $r_p(\mathbf{x}, t)$ are still given by (3.2), (3.3) and (3.5), respectively. The helicity is given by

$$\mathcal{H}(\tau) = \int \mathbf{u} \cdot \boldsymbol{\omega} dV = \int (\mathbf{u}_1 \cdot \boldsymbol{\omega}_0 + \mathbf{u}_0 \cdot \boldsymbol{\omega}_1) dV = \mathcal{H}_0(\tau) + \mathcal{H}_1(\tau), \quad \text{say.} \quad (4.9)$$

Let us first calculate $\mathcal{H}_1(\tau)$. Substituting (4.7) and (4.8) and rearranging, we obtain,

$$\mathcal{H}_1(\tau) = \frac{\Gamma^2}{2\pi^2} s(\tau) \sin \beta \iiint \frac{y}{r^2} (1 - e^{-r^2/\delta^2}) e^{-s(\tau)r_p^2/\delta^2} dx dy dz, \quad (4.10)$$

where, as before, $s(\tau) = (3 \cos^2 \beta - 1)/2$.

With the dimensionless variables $(\hat{x}, \hat{y}, \hat{z}, \hat{Y}, \hat{y}_0)$ already introduced, and with $Z = \hat{z} \sin \beta \sim \hat{z} e^{-3\tau}$ (a change of variable that reflects the increasing scale in the z -direction), (4.10) becomes

$$\mathcal{H}_1(\tau) = \frac{\Gamma^2}{2\pi^2} s(\tau) \iiint \frac{\hat{y}}{\hat{x}^2 + \hat{y}^2} (1 - e^{-(\hat{x}^2 + \hat{y}^2)}) e^{-s(\tau)[(\hat{x} \cos \beta - Z)^2 + (\hat{y} - \hat{Y})^2]} d\hat{x} d\hat{y} dZ. \quad (4.11)$$

Integration with respect to Z (from $-\infty$ to $+\infty$) gives

$$\mathcal{H}_1(\tau) = \frac{s^{1/2} \Gamma^2}{2\pi^{3/2}} \iint \frac{\hat{y}}{\hat{x}^2 + \hat{y}^2} (1 - e^{-(\hat{x}^2 + \hat{y}^2)}) e^{-s(\hat{y} - \hat{Y})^2} d\hat{x} d\hat{y}. \quad (4.12)$$

Integration with respect to \hat{x} (again from $-\infty$ to $+\infty$) is now possible. Care is needed to treat separately the cases for which \hat{y} is positive or negative, the latter being then transformed by the change of variable $\hat{y} \rightarrow -\hat{y}$; the result, after simplification, is

$$\mathcal{H}_1(\tau) = \frac{s^{1/2} \Gamma^2}{2\pi^{1/2}} \int_0^\infty \operatorname{erf} \hat{y} (e^{-s(\hat{y} - \hat{Y})^2} - e^{-s(\hat{y} + \hat{Y})^2}) d\hat{y}. \quad (4.13)$$

It is now evident from (4.13) that $\mathcal{H}_1(\tau)$ depends on τ only through the dimensionless separation $\hat{Y} = \hat{y}_0 e^{-\tau}$ and $s(\tau)$, i.e. on the instantaneous relative configuration of the two vortices, and this even when \hat{Y} is small so that they overlap. It follows that $\mathcal{H}_0(\tau) = \mathcal{H}_1(\tau)$, because we could equally have chosen coordinates with origin on B_1 and z -axis parallel to \mathbf{e} . Hence

$$\mathcal{H}(\tau) = 2\mathcal{H}_1(\tau) = \frac{s^{1/2} \Gamma^2}{\pi^{1/2}} \int_0^\infty \operatorname{erf} \hat{y} (e^{-s(\hat{y} - \hat{Y})^2} - e^{-s(\hat{y} + \hat{Y})^2}) d\hat{y}. \quad (4.14)$$

The integral (4.14) is easily evaluated using Mathematica (note that, for large \hat{Y} , the dominant contribution comes from the neighbourhood of $\hat{y} = \hat{Y}$). Figure 9 shows the result for an initial skewness angle $\beta_0 = \pi/4$, and for six values of the initial dimensionless separation \hat{y}_0 . As expected, for $\hat{y}_0 \gg 1$, \mathcal{H}/Γ^2 remains very nearly equal to 1 (as anticipated in (4.6)) for so long as the vortices are well separated; however, as $\hat{Y}(\tau)$ decreases to $O(1)$ and smaller, the helicity decays exponentially to zero in a time of order α^{-1} . (For $\hat{y}_0 \sim 1$, the initial increase of helicity is caused by the increase of the stretch rate $s(t)$ (figure 3), which decreases the cross-section of B_1 , and so decreases the extent of its overlap with B_0 ; this effect is soon more than compensated by the exponential approach ($\hat{Y} \sim e^{-\tau}$) of the vortex centrelines.)

We therefore find no evidence for helicity conservation during reconnection within the framework of our present model. On the contrary, the initial helicity is destroyed during the reconnection process. Again, of course, one may ask: ‘What if the vortex–vortex interaction terms are retained in this model problem? Can twist, and so helicity, be generated by vortex–vortex interaction?’ To address this, a perturbation procedure taking first-order account of the interaction terms might provide an answer; alternatively, a full numerical simulation of the 3D time-dependent Navier–Stokes equations could in principle be carried out for the trefoil configuration, but this would no doubt run into the unsolved and deeply challenging finite-time singularity problem. In the meantime, all that can be said is that the linearised model described in this paper provides no evidence for conservation of helicity during viscous reconnection of vortex tubes.

We note finally that the model is much more reliable in the magnetic context, in which the magnetic analogue of (2.2) is exact in the weak magnetic field limit in which Lorentz forces are negligible. Our conclusion here is that magnetic helicity is not conserved under diffusive reconnection of magnetic flux tubes.

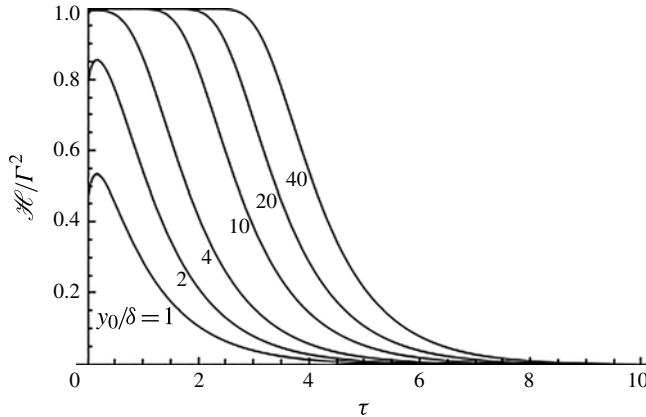


FIGURE 9. Dimensionless helicity \mathcal{H}/Γ^2 as a function of dimensionless time $\tau = \alpha t$ for the skewed vortices B_0 and B_1 driven together by the strain field (2.1), as evaluated from (4.14) for $\beta_0 = \pi/4$ and six values of the initial dimensionless separation $\hat{y}_0 = y_0/\delta$. For $\hat{y}_0 \gg 1$, the helicity remains constant until the vortices overlap, and then decays to zero exponentially in a time of order α^{-1} .

Acknowledgements

This work was initiated during the programme Topological Dynamics in the Physical and Biological Sciences at the Isaac Newton Institute (July–December 2012), and we are grateful to the Director and Staff of the Institute for hospitality and support during this programme. We thank W. Irvine for stimulating discussions and for permitting reproduction of the clips in figure 1; and we acknowledge the comments of two referees, which have led to substantial improvements in presentation.

Appendix A. Burgers vortex convected by non-axisymmetric strain

With the general non-axisymmetric strain (1.1), the linearised vorticity equation takes the form

$$\frac{\partial \boldsymbol{\omega}}{\partial t} = \alpha x \frac{\partial \boldsymbol{\omega}}{\partial x} + \beta y \frac{\partial \boldsymbol{\omega}}{\partial y} + (\alpha + \beta) \boldsymbol{\omega} + \nu \left(\frac{\partial^2 \boldsymbol{\omega}}{\partial x^2} + \frac{\partial^2 \boldsymbol{\omega}}{\partial y^2} \right). \tag{A 1}$$

It is well known that the non-axisymmetric Burgers vortex

$$\boldsymbol{\omega}_B(x, y) = (\Gamma/\pi\delta_x\delta_y) \exp[-(x^2/\delta_x^2 + y^2/\delta_y^2)] \tag{A 2}$$

with $\delta_x = \sqrt{2\nu/\alpha}$ and $\delta_y = \sqrt{2\nu/\beta}$, is a steady solution of this equation (but not, unless $\alpha = \beta$, an exact solution of the nonlinear Navier–Stokes equation).

If a vortex of this type is initially centred at (x_0, y_0) , then by time t its centre will have moved to $(x_0 e^{-\alpha t}, y_0 e^{-\beta t})$. We may therefore assert (cf. (2.4)) that

$$\begin{aligned} \omega(x, y, t) &= \omega_B(x - x_0 e^{-\alpha t}, y - y_0 e^{-\beta t}) \\ &= \frac{\Gamma}{\pi\delta_x\delta_y} \exp \left[- \left(\frac{(x - x_0 e^{-\alpha t})^2}{\delta_x^2} + \frac{(y - y_0 e^{-\beta t})^2}{\delta_y^2} \right) \right] \end{aligned} \tag{A 3}$$

is a solution of (A 1). This may be verified directly. For, from (A 3),

$$\frac{\partial \omega}{\partial t} = -2 \left[\frac{\alpha x_0}{\delta_x^2} (x - x_0 e^{-\alpha t}) + \frac{\beta y_0}{\delta_y^2} (y - y_0 e^{-\beta t}) \right] \omega. \quad (\text{A } 4)$$

Also,

$$\frac{\partial \omega}{\partial x} = -\frac{2(x - x_0 e^{-\alpha t})}{\delta_x^2} \omega, \quad \frac{\partial^2 \omega}{\partial x^2} = \left(-\frac{2}{\delta_x^2} + \frac{4(x - x_0 e^{-\alpha t})^2}{\delta_x^4} \right) \omega; \quad (\text{A } 5a, b)$$

hence, after some simplification,

$$\alpha x \frac{\partial \omega}{\partial x} + \alpha \omega + \nu \frac{\partial^2 \omega}{\partial x^2} = -2 \left[\frac{\alpha x_0}{\delta_x^2} (x - x_0 e^{-\alpha t}) \right] \omega, \quad (\text{A } 6)$$

and, similarly,

$$\beta y \frac{\partial \omega}{\partial y} + \beta \omega + \nu \frac{\partial^2 \omega}{\partial y^2} = -2 \left[\frac{\beta y_0}{\delta_y^2} (y - y_0 e^{-\beta t}) \right] \omega. \quad (\text{A } 7)$$

Comparing (A 4), (A 6) and (A 7), it is evident that (A 3) does indeed satisfy (A 1) as expected.

Note that, with $\hat{x} = x/\delta_x$ and $\hat{x}_0 = x_0/\delta_x$, we have the Taylor expansion

$$\exp[-(\hat{x} - \hat{x}_0 e^{-\alpha t})^2] = \sum_{n=0}^{\infty} \frac{\hat{x}_0^n e^{-n\alpha t}}{n!} e^{-\hat{x}^2} H_n(\hat{x}), \quad (\text{A } 8)$$

where

$$H_n(x) = (-1)^n e^{x^2} \frac{d^n}{dx^n} e^{-x^2}, \quad (\text{A } 9)$$

the Hermite polynomial of order n ; similarly, for $\exp[-(\hat{y} - \hat{y}_0 e^{-\beta t})^2]$ (with $\hat{y} = y/\delta_y$ and $\hat{y}_0 = y_0/\delta_y$). Thus the solution (A 3) may be expanded as the double sum

$$\omega(x, y, t) = \frac{\Gamma}{\pi \delta_x \delta_y} \sum_{n=0}^{\infty} \sum_{m=0}^{\infty} \frac{\hat{x}_0^n \hat{y}_0^m e^{-(n\alpha t + m\beta t)}}{n! m!} e^{-(\hat{x}^2 + \hat{y}^2)} H_n(\hat{x}) H_m(\hat{y}), \quad (\text{A } 10)$$

each term being separately a solution of (A 1).

Appendix B. Effect of axial velocity in vortex cores

We consider here the addition to the Burgers vortex of an axial component of velocity $(0, 0, w(x, y, t))$, which evolves under the effect of the strain field (2.1) according to the equation

$$\frac{\partial w}{\partial t} - \alpha x \frac{\partial w}{\partial x} - \alpha y \frac{\partial w}{\partial y} = \nu \left(\frac{\partial^2 w}{\partial x^2} + \frac{\partial^2 w}{\partial y^2} \right), \quad (\text{B } 1)$$

or equivalently

$$\frac{\partial w}{\partial t} - \alpha \left(\frac{\partial(xw)}{\partial x} + \frac{\partial(yw)}{\partial y} \right) + 2\alpha w = \nu \left(\frac{\partial^2 w}{\partial x^2} + \frac{\partial^2 w}{\partial y^2} \right). \quad (\text{B } 2)$$

There is no pressure-gradient contribution in this equation because $\partial w/\partial z = 0$.

We assume that $w(x, y, t)$ is exponentially small for large $r^2 = x^2 + y^2$. Let

$$Q(t) = \int w(x, y, t) \, dx \, dy, \quad (\text{B } 3)$$

the axial flux within the vortex. Integrating (B 2) over the (x, y) -plane, we immediately have that $dQ/dt + 2\alpha Q = 0$, so that this axial flux decays exponentially:

$$Q(t) = Q_0 e^{-2\alpha t}. \quad (\text{B } 4)$$

It is then not difficult to show that (B 2) admits a corresponding solution

$$w(x, y, t) = (Q_0/\pi\delta^2) e^{-2\alpha t} e^{-r^2/\delta^2}, \quad (\text{B } 5)$$

where still $\delta^2 = 2\nu/\alpha$. When combined with the Burgers solution (2.3), the vortex lines become helices, which are stretched in the z -direction (with pitch increasing like $e^{2\alpha t}$) while being simultaneously subject to radial diffusion (cf. the ‘strained spiral vortex’ underlying Lundgren’s (1982) model of turbulent fine structure). This combined solution provides a helical generalisation of the Burgers vortex, also an exact (albeit unsteady) solution of the Navier–Stokes equation.

REFERENCES

- BORATAV, O. N., PELZ, R. B. & ZABUSKY, N. J. 1992 Reconnection in orthogonally interacting vortex tubes: direct numerical simulations and quantifications. *Phys. Fluids A* **4**, 581–605.
- BUNTINE, J. D. & PULLIN, D. I. 1989 Merger and cancellation of strained vortices. *J. Fluid Mech.* **205**, 263–295.
- BURGERS, J. M. 1948 A mathematical model illustrating the theory of turbulence. *Adv. Appl. Mech.* **1**, 171–199.
- DOUADY, S., COUDER, Y. & BRACHET, M. E. 1991 Direct observation of the intermittency of intense vorticity filaments in turbulence. *Phys. Rev. Lett.* **67**, 983–986.
- HATTORI, Y. & MOFFATT, H. K. 2005 Reconnexion of vortex and magnetic tubes subject to an imposed strain: an approach by perturbation expansion. *Fluid Dyn. Res.* **26**, 333–356.
- HUNT, J. C. R. & CARRUTHERS, D. J. 1990 Rapid distortion theory and the ‘problems’ of turbulence. *J. Fluid Mech.* **212**, 497–532.
- ISHIHARA, T., KANEDA, Y., YOKOKAWA, M., ITAKURA, K. & UNO, A. 2007 Small-scale statistics in high-resolution direct numerical simulation of turbulence: Reynolds number dependence of one-point velocity gradient statistics. *J. Fluid Mech.* **592**, 335–366.
- KERR, R. M. 2013 Swirling, turbulent vortex rings formed from a chain reaction of reconnection events. *Phys. Fluids* **25**, 065101.
- KIDA, S. & TAKAOKA, M. 1987 Bridging in vortex reconnection. *Phys. Fluids* **30**, 2911–2914.
- KIDA, S. & TAKAOKA, M. 1994 Vortex reconnection. *Annu. Rev. Fluid Mech.* **26**, 169–189.
- KIMURA, Y. & KOIKARI, S. 2004 Particle transport by a vortex soliton. *J. Fluid Mech.* **510**, 201–218.
- KLECKNER, D. & IRVINE, W. T. M. 2013 Creation and dynamics of knotted vortices. *Nat. Phys.* **9**, 253–258; see also <http://www.newton.ac.uk/programmes/TOD/seminars/2012091111302.html>.
- KUDELA, H. & KOSIOR, A. 2013 Parallel computation of vortex tube reconnection using a graphics card and the 3D vortex-in-cell method. *Proc. IUTAM* **7**, 59–66.
- LUNDGREN, T. S. 1982 Strained spiral vortex model for turbulent fine structure. *Phys. Fluids* **25**, 2192–2203.
- MELANDER, M. V. & HUSSAIN, F. 1989 Cross-linking of two antiparallel vortex tubes. *Phys. Fluids A* **1**, 633–636.
- MOFFATT, H. K. 1969 The degree of knottedness of tangled vortex lines. *J. Fluid Mech.* **35**, 117–129.

- MOFFATT, H. K. & HUNT, R. E. 2002 A model for magnetic reconnection. In *Tubes, Sheets and Singularities in Fluid Dynamics* (ed. H. K. Moffatt & K. Bajer), pp. 125–138. Kluwer.
- MOFFATT, H. K., KIDA, S. & OHKITANI, K. 1994 Stretched vortices – the sinews of turbulence; large-Reynolds-number asymptotics. *J. Fluid Mech.* **259**, 241–264.
- MOFFATT, H. K. & RICCA, R. L. 1992 Helicity and the Călugăreanu invariant. *Proc. R. Soc. Lond. A* **439**, 411–429.
- PRIEST, E. R. & FORBES, T. 2000 *Magnetic Reconnection*. Cambridge University Press.
- PULLIN, D. I. & SAFFMAN, P. G. 1998 Vortex dynamics in turbulence. *Annu. Rev. Fluid Mech.* **30**, 31–51.
- VAN REES, W. M., HUSSAIN, F. & KOUMOUTSAKOS, P. 2012 Vortex tube reconnection at $Re = 104$. *Phys. Fluids* **24**, 075105.
- ROTT, N. 1958 On the viscous core of a line vortex. *Z. Angew. Math. Phys.* **9**, 543–553.
- TAYLOR, J. B. 1974 Relaxation of toroidal plasma and generation of reverse magnetic fields. *Phys. Rev. Lett.* **33**, 1139–1141.
- SAFFMAN, P. G. 1990 A model of vortex reconnection. *J. Fluid Mech.* **212**, 395–402.
- TOWNSEND, A. A. 1951 On the fine-scale structure of turbulence. *Proc. R. Soc. Lond. A* **208**, 534–542.
- VINCENT, A. & MENEGUZZI, M. 1991 The spatial structure and statistical properties of homogeneous turbulence. *J. Fluid Mech.* **225**, 1–25.
- WRIGHT, A. N. & BERGER, M. A. 1989 The effect of reconnection upon the linkage and interior structure of magnetic flux tubes. *J. Geophys. Res. Space Phys.* **94**, 1295–1302.